CrystEngComm

PAPER

View Article Online
View Journal | View Issue

Cite this: *CrystEngComm*, 2016, **18**, 2830

Exploring the effect of poly(acrylic acid) on pre- and post-nucleation $BaSO_4$ species: new insights into the mechanisms of crystallization control by polyelectrolytes†

Cristina Ruiz-Agudo,*[a] Encarnación Ruiz-Agudo,[b] Alejandro Burgos-Cara,[b] Christine V. Putnis,[ac] Aurelia Ibáñez-Velasco,[b] Carlos Rodriguez-Navarro[b] and Andrew Putnis[ad]

Received 20th January 2016,
Accepted 29th February 2016

DOI: 10.1039/c6ce00142d

www.rsc.org/crystengcomm

Barium sulphate ($BaSO_4$) precipitation has been suggested to occur by non-classical pathways that include the formation of a dense liquid precursor phase, nucleation of primary nanoparticles and two levels of oriented aggregation resulting in micron-sized barite single crystals. In this study we build from this previous knowledge and explore how Ba^{2+} and SO_4^{2-} ions associate in solution prior to nucleation of a solid phase and the effects of poly(acrylic acid) (PAA) in these pre-nucleation and post-nucleation stages. With this aim, *in situ* potentiometric experiments and transmission electron microscopy (TEM) observations of time-resolved quenched samples were carried out. Additional bulk precipitation experiments in which supersaturation was achieved by rapid mixing of Ba- and SO_4-bearing solutions were performed. The resultant precipitates were characterized by scanning electron microscopy (FESEM and ESEM), transmission electron microscopy (TEM), X-ray diffraction (XRD) and thermogravimetric (TG) analyses. Our study provides evidence that barium sulphate precipitation occurs *via* the formation of ion associates in solution (ion pairs and/or clusters), that are significantly destabilized in the presence of PAA. This is associated with a noticeable delay in nucleation in the presence of PAA. Thus, our results provide indirect evidence that suggests that prenucleation ion associates must form prior to solid $BaSO_4$ nucleation. Alternatively, $BaSO_4$ mineralization in the presence of PAA seems to occur by a different route that consists in the formation of Ba-PAA globules in solution followed by an amorphous hydrated $BaSO_4$ phase that transform into crystalline barite nanoparticles. PAA seems to stabilize this amorphous phase, which nevertheless also forms in the absence of PAA. Finally, single micron-sized crystals are formed by the oriented attachment of distinguishable smaller subunits, thus forming mesocrystals in the presence and absence of PAA.

Introduction

Barium sulphate scale formation causes significant problems in the oil recovery industry. Barite scale deposits form due to the mixing of seawater (high sulphate content) and formation water (high barium content) during oil recovery. Solid layers of barite can precipitate in the pipes and/or in the pores of the reservoir rocks and this can affect oil production by restricting fluid flow. Barite scale is hard, adherent and difficult to remove and its formation can lead to an additional increase in operating costs.[1,2] A common strategy to reduce scale formation is the addition of organic additives to the seawater injected in the reservoir to inhibit barite nucleation or growth. Thus a better understanding of the mechanism of barite formation from aqueous solutions and the influence of additives may help in the design of more effective strategies for barite scale prevention. Additionally, the study of $BaSO_4$ precipitation in aqueous solutions and the interaction with organic molecules is also relevant because barite ubiquitously appears in marine sediments and in the water column in association with organic matter, and its major and trace element signature has been used as an archive of the chemistry of the seawater from which it precipitated. Carboxyl groups in the structural polymers of the membrane cell wall of bacteria are thought to play an important role in marine barite precipitation process.[3] Thus knowledge of barite formation

[a] *Institut für Mineralogie, Corrensstrasse 24, 48149 Münster, Germany. E-mail: c_ruiz02@uni-muenster.de*
[b] *Department of Mineralogy and Petrology, University of Granada, 18071, Spain*
[c] *Nanochemistry Research Institute, Department of Chemistry, Curtin University, 6845 Perth, Australia*
[d] *The Institute of Geoscience Research (TIGeR), Curtin University, Perth, Australia*
† Electronic supplementary information (ESI) available. See DOI: 10.1039/c6ce00142d

pathways and the role of organic macromolecules at directing such processes may be relevant for understanding barite biomineralization and a more accurate use of barite composition as a proxy for past seawater chemistry.

A recent experimental study has allowed us to identify a previously unreported mechanism of $BaSO_4$ precipitation.[4] This mechanism is based on the initial formation of a liquid precursor that precedes barite single crystal formation *via* the oriented aggregation of nanoparticles and a mesoscopic transformation of these self-assembled precursor entities.[4] This occurs both in pure solutions and in solutions that contain polymeric additives. Although the transformation of mesocrystals to single crystals is especially difficult to observe in systems without stabilizing molecules, our previous time-resolved study showed significant evidence of such a transformation in the $BaSO_4$–H_2O system.

The development of more effective inhibition treatments requires a detailed characterization of barium sulphate precipitation, including the prenucleation regime and the existence of amorphous precursor phases. However, in our previous work it was not possible to unambiguously discern the amorphous or crystalline nature of the precursor material. Amorphous precursors are metastable with respect to the corresponding crystalline polymorph and frequently, in systems where their life-time is short, such species are overlooked.[5] Amorphous calcium carbonate and amorphous calcium phosphate can be relatively stable in solution; this is why they have been frequently isolated and characterized.[6,7] Amorphous barium-bearing phases may be significantly less stable than those containing Ca or Mg, due to the strongly hydrated character of Ca^{2+} and Mg^{2+} compared to Ba^{2+}, as deduced from the values of the free energy of hydration (−1820, −1493 and −1238 kJ mol^{-1} for Mg^{2+}, Ca^{2+} and Ba^{2+}, respectively).[8] The formation of anhydrous crystalline phases from amorphous precursor phases requires water molecules to be expelled and this process has a higher energy cost for strongly hydrated ions (Ca^{2+} and Mg^{2+}).[9] This would result in the formation of more "stable" amorphous precursor phases when strongly hydrated ions are involved making them easier to detect. High vacuum conditions and the use of highly energetic electron beams for the analysis and observation of the early stages of barite formation in previous studies may have triggered an amorphous to crystalline transition, thus making the identification of amorphous barium sulphate phases difficult. In fact, to our knowledge there is only one study reporting the formation of amorphous barium sulphate and it occurs in the presence of an organic compound.[10]

Using the insights from our early work, we have investigated the initial stages of the precipitation of barium sulphate in organic- and salt-free solutions to identify the precipitation pathway and to look for any potential precursor phase(s) of crystalline barite. Furthermore, we explore the use of poly(acrylic acid) (PAA) to control the precipitation of barium sulphate. The effect of additives on barite precipitation has been extensively studied by Cölfen and coworkers.[11–14] Here we show that organic additives are also effective at modifying pre-nucleation stages of barite precipitation.

PAA is an example of a polymeric scale inhibitor,[15] that is, an additive used to avoid or retard mineral precipitation and it is also regarded as a synthetic analogue of the highly acidic macromolecules present within many biominerals.[16] It has been shown in recent years that polymers induce the formation of liquid precursors phases (*i.e.* PILPs)[17] that can be moulded into non-equilibrium shapes such as the morphologies found in biominerals. Thus, understanding how polymers interact with ions or with prenucleation species can shed light onto the formation of biominerals. Furthermore, amorphous precursor phases can be stabilized by some organic molecules which hinder or delay the transformation into more stable crystalline phases.[18] PAA is known to increase the long-term stability of precursor phases in systems such as $CaCO_3$–H_2O (ref. 5) or $CaSO_4$–H_2O.[19] In this study, we demonstrate that barite can precipitate from pure (*i.e.*, additive-free) solutions at room temperature *via* the formation of ion associates (ion pairs and/or clusters) followed by an intermediate hydrated amorphous barium sulphate phase. PAA increases the stability of such a precursor, thus allowing observation of its formation. Our results provide another piece of evidence of the formation of ion associates and precursor phases preceding the stable crystalline phase, suggesting that this may be a universal phenomenon during the precipitation of inorganic compounds. Furthermore, this study provides confirmation of the particle-based crystallization of barium sulphate, including oriented attachment and mesocrystal formation processes, both in the presence and in the absence of organics.

Materials and methods

Titration experiments

Precipitation experiments were performed using a commercially available titration setup manufactured by Methrom, in a jacketed vessel at controlled temperature (20.0 ± 0.2 °C) and under continuous stirring. Na_2SO_4 and $BaCl_2$ solutions were prepared from 1 M stock solutions made from solids from Merck Suprapur min. 99.995% ($BaCl_2$), Sigma Aldrich min. 99% (Na_2SO_4) and doubly deionized water (Milli-Q, resistivity >18.2 MΩ cm). The polyacrylic acid (Sigma Aldrich, $C_3H_3Na0_2$) used has an averaged molar mass of 2100 g mol^{-1}, *i.e.*, one molecule PAA provides approximately 22 carboxylic acid groups. A 10 mM $BaCl_2$ solution was continuously added to 1 mM Na_2SO_4 at a rate of 60 μl min^{-1}. Ba^{2+} potential was monitored by means of an ion selective electrode (ISE, Mettler-Toledo, DX337-Ba). The pH was measured using a glass electrode from Methrom that served as well as the reference for the Ba-ISE. Conductivity measurements were performed with 856 conductivity module (Metrohm) and transmittance was monitored with Optrode sensor for titration using wavelength of 520 nm (Metrohm). After each experiment, the reaction vessel, the burette tips and the electrodes were washed using a 10 mM EDTA solution at pH

11 to remove any Ba^{2+} and subsequently washed with water (Milli-Q).

Stepwise addition of $BaCl_2$ to doubly deionized water (Milli-Q) was performed for calibration of the Ba-ISE. In these calibration runs, Ba^{2+} potential was measured as a function of solution concentration, using identical settings as in the precipitation runs. Calibration was conducted in water because the ionic strengths in the different precipitation runs are low and the ionic activity contribution is within the range of the typical experimental error. This results in a sustainable approximation.[20] Barium potentials in the experimental runs were converted into free barium concentrations using an average linear equation determined in the calibration assays in water. Inductively coupled plasma optical emission spectrometry (ICP-OES) was used to analyse Ba in the $BaCl_2$ solutions added in our experiments for accurate determination of the amount of barium dosed. Since the volume added to the reaction vessel is known at all times, free barium can be calculated from these concentrations. Concentrations of PAA ranging from 0 to 50 mg l^{-1} were added to the Na_2SO_4 solution. This titration-based setup has been recently used to gain detailed insights into the nucleation of sparingly soluble carbonates ($CaCO_3$ (ref. 21) and $BaCO_3$ (ref. 22)) and to quantitatively assess the multiple effects of additives on the early stages of nucleation and growth of such minerals.[23]

In the course of selected experimental runs, aliquots of the reaction solution were withdrawn from the reaction vessel at different reaction intervals, quenched in ethanol and particles were collected for transmission electron microscopy (TEM) observations by dipping carbon film coated copper grids into the alcohol dispersions. TEM and HRTEM analysis of particles were carried out using a Philips CM20, operated at 200 kV and a FEI Titan, operated at 300 kV. TEM observations were performed using a 40 μm (CM20) or a 30 μm (Titan) objective aperture. SAED patterns were collected using a 10 μm aperture allowing collection of diffraction data from a circular area *ca.* 0.2 μm in diameter. Compositional maps of selected areas were acquired in scanning transmission electron microscopy (STEM) mode using a Super X EDX detector (FEI), formed by four windowless SSD detectors. STEM images in the FEI Titan TEM of the areas analysed by EDX were collected with a high angle annular dark field (HAADF) detector. After the completion of the titration experiments, the solids were filtered through cellulose nitrate membrane filters (Millipore pore size = 0.10 μm) and characterized by X-ray diffraction (XRD) and scanning electron microscopy (SEM).

Bulk precipitation experiments

In an additional set of experiments, barium sulphate was precipitated from aqueous solutions at room temperature by rapid mixing of equimolar solutions of $Ba(OH)_2$ and H_2SO_4 to give final Ba^{2+} and SO_4^{2-} concentrations of 1.25 mM. Solutions were prepared using reagent grade reactants from Sigma Aldrich and doubly-deionized Milli-Q water. The precipitation process was quenched at times ranging from 0 up to 1 h by quick immersion in liquid nitrogen and subsequent freeze-drying. Such a method has been used to obtain dry, counter-ion free barium sulphate in order to generate larger quantities for structural and compositional analysis.[24] As the amount of precipitate obtained in this method is higher than in titration experiments, it was possible to run full characterization of the solids by thermogravimetric analysis (TGA), XRD, and by environmental scanning electron microscopy (ESEM). TGA was performed on a Mettler-Toledo model TGA/DSC. About 10–20 mg of the sample were deposited on Pt crucibles and analyzed under flowing nitrogen (100 mL min^{-1}) at 10 °C min^{-1} heating rate, from room T up to 950 °C. Additionally, solids were deposited on zero-background Si sample holders and analyzed on a PANanalytical X'Pert Pro X-ray diffractometer equipped with Cu Kα radiation (λ = 1.5405 Å) at 2θ range between 3 and 70° and at a scanning rate of 0.002° 2θ s^{-1}. Solids were observed at high magnification by means of scanning electron microscopy (FESEM; Zeiss SUPRA40VP and ESEM; Phillips Quanta) and transmission electron microscopy (TEM) using a Philips CM20, operated at 200 kV and a FEI Titan, operated at 300 kV. Prior to TEM observations, freeze-dried solids were re-suspended in ethanol and deposited on carbon film coated copper grids.

Results

Potentiometric analysis of barium sulphate precipitation

Fig. 1 shows the time evolution of free-Ba^{2+} concentration (blue curve in Fig. 1a) and transmittance (grey curve in Fig. 1a) during a control run in which no PAA was used. The full black line is the rate at which Ba^{2+} ions are added to the solution. In the control experiments, free Ba^{2+} concentration increases with time, until a maximum is reached and nucleation of $BaSO_4$ occurs. The free Ba^{2+} concentration in solution then drops and progressively approaches a constant level that is related to the solubility of the precipitated phase.[21] At small added Ba^{2+} values, the observed offset in the temporal increase in free-Ba^{2+} prior to nucleation relative to the total amount of Ba^{2+} added may be attributed to Ba^{2+} pairing with SO_4^{2-} to form $BaSO_4$ pairs. Approximately between 70 and 80% of the added barium is bound at the nucleation point. The free-Ba^{2+} plot after the nucleation event shows different slopes that are related to different rates of barium removal from the aqueous media during the precipitation process (Fig. 1). The waiting time for nucleation was found to be 700 ± 90 s. Similarly, the conductivity increases more or less linearly up to the nucleation point and then decreases also linearly until it reaches a constant level; after that, it starts to rise again (green curve, Fig. 1b). The "conductivity plateau" is reached before the "free-Ba^{2+} plateau" and it corresponds to a change in the slope of the free-Ba^{2+} curve. The transmittance (Fig. 1a) remains approximately constant from the beginning of the experiments until nucleation occurs and then it drops to a constant level at the end of the precipitation process. Fig. 1a shows that the point at which transmittance drops approximately coincides with the point at which the

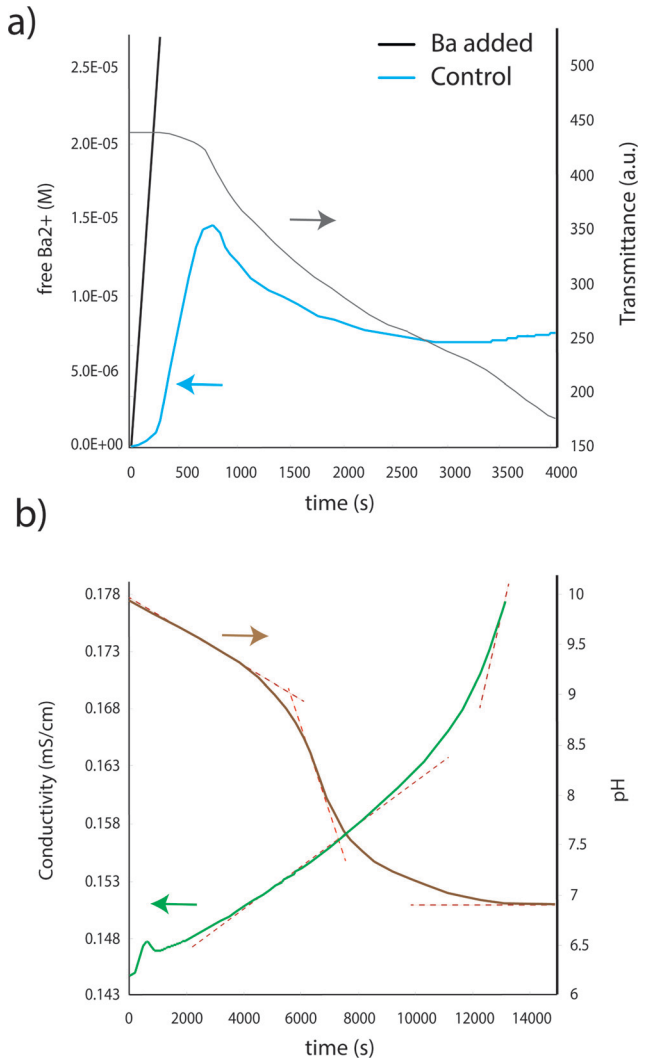

Fig. 1 a) Time development of the amount of free Ba^{2+}-ions in the control run (blue line). Note that during the prenucleation stage (up to *ca.* 900 s) less Ba^{2+} is detected than added (black line), which can be associated with the binding of ions in prenucleation clusters. The evolution of transmittance in the control is also represented (grey line). b) Evolution of conductivity (green line) and pH (brown line) in the control run.

free-Ba^{2+} concentration drops in PAA-free control experiments. The pH curve in the control runs of the solution decreases continuously during the experiments, showing three distinct parts with different slopes (brown curve, Fig. 1b).

From conductivity and ISE measurements, the amount of sulphate and barium bonded in the prenucleation stage (Fig. S1, ESI†) can be independently assessed. Assuming that prenucleation ion associates are neutral (*i.e.*, a 1 : 1 barium to sulphate ratio in the associates), our calculations show that the total amounts of bound sulphate (calculated from conductivity measurements) and bound barium (calculated from ISE measurements) agree well within experimental error, thus indicating that prenucleation associates are indeed neutral as assumed for the calculations.

The evolution of free-Ba^{2+} measured in solution in the presence of different PAA concentrations (0, 1, 2.5, 5, and 50 mg l^{-1}) is shown in Fig. 2a. The point at which transmittance drops as indicated by the bend in the grey dotted line has been also included. For the sake of clarity, in Fig. 2b only the plot of the evolution of free-Ba^{2+} concentration in solution and transmittance for 2.5 mg l^{-1} of PAA is given. Here a noticeable delay between the drop in transmittance and the drop in the free Ba^{2+} concentration measured in the presence of PAA can be observed. Furthermore, a closer look at this curve (Fig. S2, ESI†) shows that, after the nucleation point (free-Ba^{2+} onset), the curve shows different slopes that could be related to different stages of the precipitation process, as stated above for the control runs. Regarding the conductivity evolution in the presence of PAA (Fig. S2, ESI†), it was found that the conductivity curve starts to bend when the maximum in free Ba^{2+} is reached, but its drop coincides with the drop in transmittance. The "conductivity plateau" is reached

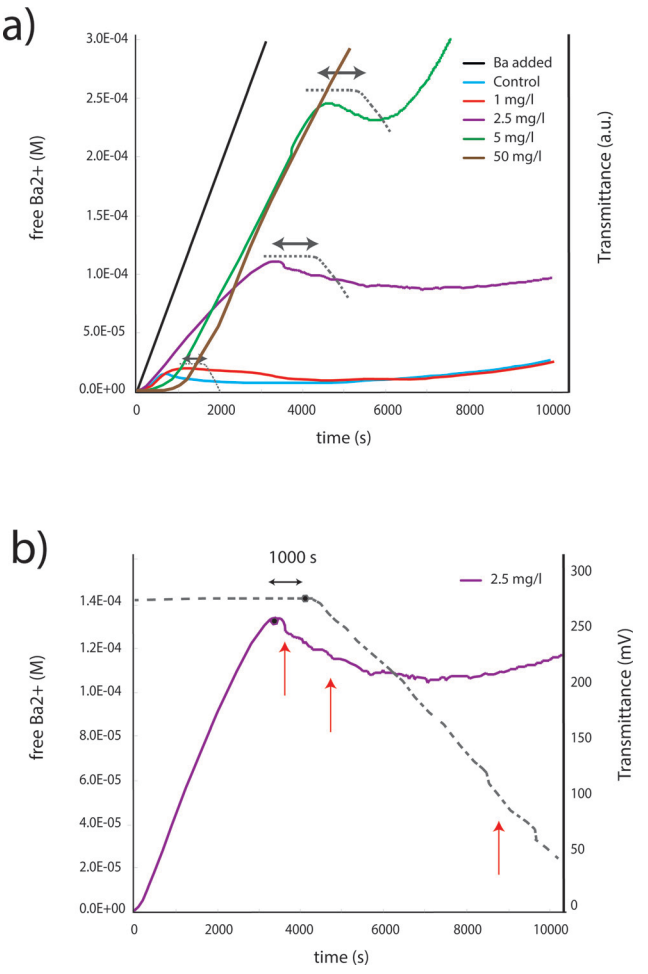

Fig. 2 a) Time development of the amount of free Ba^{2+}-ions in the presence of different amounts of PAA. The black line refers to the amount of Ba^{2+} added. Schematic evolution of transmittance is also represented (grey dotted line). b) Evolution of free-Ba^{2+} and transmittance when 2.5 mg l^{-1} of PAA were tested. Red arrows indicate the time points at which the respective aliquots were taken and isolated.

before the free-Ba^{2+} plateau, and subsequently conductivity increases at two different rates as deduced from the two different slopes observed in the conductivity curves (in a similar way as in the control runs).

The comparison of the titration curves obtained in the absence and in the presence of PAA shows significant differences in the offset and the slope of the time evolution of the free-Ba^{2+} concentration in solution prior to nucleation, the time of nucleation (*i.e.*, waiting time), and the level of the free-Ba^{2+} in solution after nucleation. Changes in these parameters relative to the reference experiments can be seen as a function of PAA concentration in Fig. 3. First, it can be seen that the addition of PAA increases the extent of the offset in the time development of the measured barium free concentration in solution (Fig. 3a). From the intercept with the *x*-axis, we can estimate an average binding capacity of the PAA of ~0.21 barium ions per PAA molecule, or one barium ion to *ca.* 5 carboxylic acid groups. To evaluate such binding between Ba^{2+} and PAA individually (without the interference of sulphate) we carried out another series of experiments in which 10 mM $BaCl_2$ was continuously added to Milli-Q water with different PAA concentration (0, 10, 20 and 50 mg l^{-1}). Our results show that there is a detectable binding of Ba^{2+} by PAA in the absence of sulphate (Fig. S3a, ESI†). Comparison between the binding capacity of PAA in water and in 1 mM sulphate solution shows no detectable effect of sulphate on the binding capacity of PAA (Fig. S3b, ESI†).

Additionally, it was observed that increasing the PAA concentration in the sodium sulphate solution leads to a progressive steepening of the linear part of free-Ba^{2+} concentration curves prior to nucleation (Fig. 3b). This is associated with a noticeable delay in nucleation, which also increases with PAA concentration (Fig. 3b). Finally, PAA also influences the free-Ba^{2+} concentration measured after nucleation, which is higher in all PAA-bearing runs than in the reference runs (no PAA in the sulphate solution). In fact, the free barium concentration measured in the 5 mg l^{-1} PAA sample exceeds that of the control run by a factor of approximately 40 (Fig. 3c).

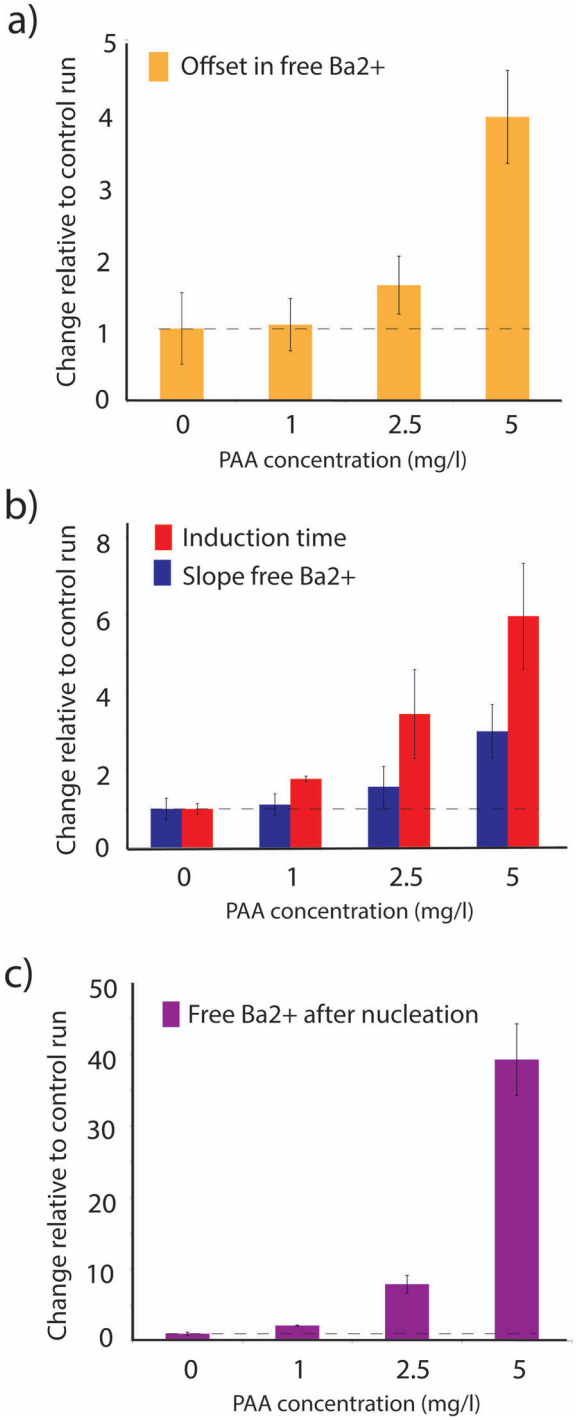

Fig. 3 Bar plots illustrating the effect of added PAA on (a) the offset of the time evolution of the free-Ba^{2+} concentration in solution prior to nucleation; (b) the induction time and slope of free-Ba^{2+} concentration prior to nucleation; (c) and the level of the free-Ba^{2+} in solution after nucleation. Results are given as relative changes to the PAA-free reference experiments (control run).

Characterization of particle evolution in titration experiments

Aliquots of the reaction media were quenched in ethanol at different reaction times (marked by red arrows in Fig. 2b) for the 2.5 mg l^{-1} PAA run. The first sample was taken at a point in which the free-Ba^{2+} concentration measured was already decreasing but the transmittance of the solution remained unaltered (region I in Fig. S2, ESI†). TEM analysis shows the presence of rounded structures in which only barium, carbon and oxygen are detected by EDX (see the spectrum shown in the upper left corner of Fig. 4). In the HAADF image it can be seen that these globular structures exhibit a brighter central part surrounded by a darker area (Fig. 4 and Fig. S4, ESI†). The brightness in HAADF images is related to the average atomic number; thus, it seems feasible that barium is concentrated in the central part of these structures. These globules are amorphous (see the SAED pattern in the lower right corner of Fig. 4), and the EDX elemental maps collected in some of these globules (Fig. S4, ESI†) confirm that barium is concentrated in the globules while sulphur is equally distributed all over the grid (*i.e.*, values corresponded to those of

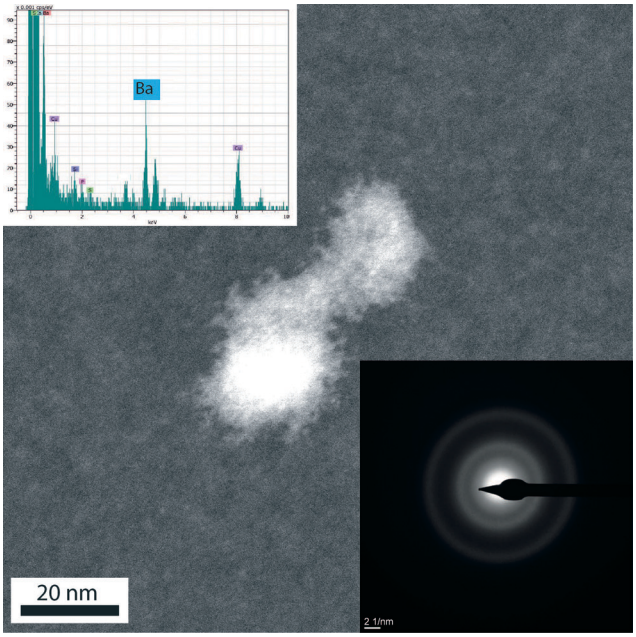

Fig. 4 STEM-HAADF image of a Ba-PAA globule obtained after the isolation of an aliquot at the first stage in 2.5 mg l^{-1} PAA titration experiment (first red arrow in Fig. 2). Only barium, carbon and oxygen are detected by EDX (inset in the upper left corner). The SAED pattern in the lower right corner confirms the amorphous character of these globules.

the background, which implies that the actual S concentration is nearly at the limit of detection).

The second sample was collected when both the free-Ba^{2+} concentration and the transmittance of the solution were decreasing. At this stage, we observe oval-shaped particles of approx. 100 nm (Fig. 5a) and also shapeless structures (~20 up to ~100 nm in size) with poorly-defined contours (Fig. 5b), whose EDX analysis shows both barium and sulphur peaks (Fig. S5, ESI†). The SAED patterns of these particles (insets in Fig. 5a and b) show diffraction spots superimposed to diffuse halos that indicate the presence of amorphous material. Note that the supporting C film does not present such halos. Polycrystallinity is observed in both SAED patterns. Finally, an additional sample was collected when transmittance and free-Ba^{2+} curves were approaching a constant level after nucleation (third arrow in Fig. 2b). Ellipsoidal particles of barite (~700 nm in size) that diffract as single crystals are observed at this stage (Fig. 6). These particles are formed by smaller subunits (nanoparticles; ~5 to 10 nm in size); low e-absorbing areas are visible within these nanoparticles and they could correspond to empty spaces between nanoparticles in which PAA concentrates. EDX analysis and SAED patterns confirm that these particles are barite.

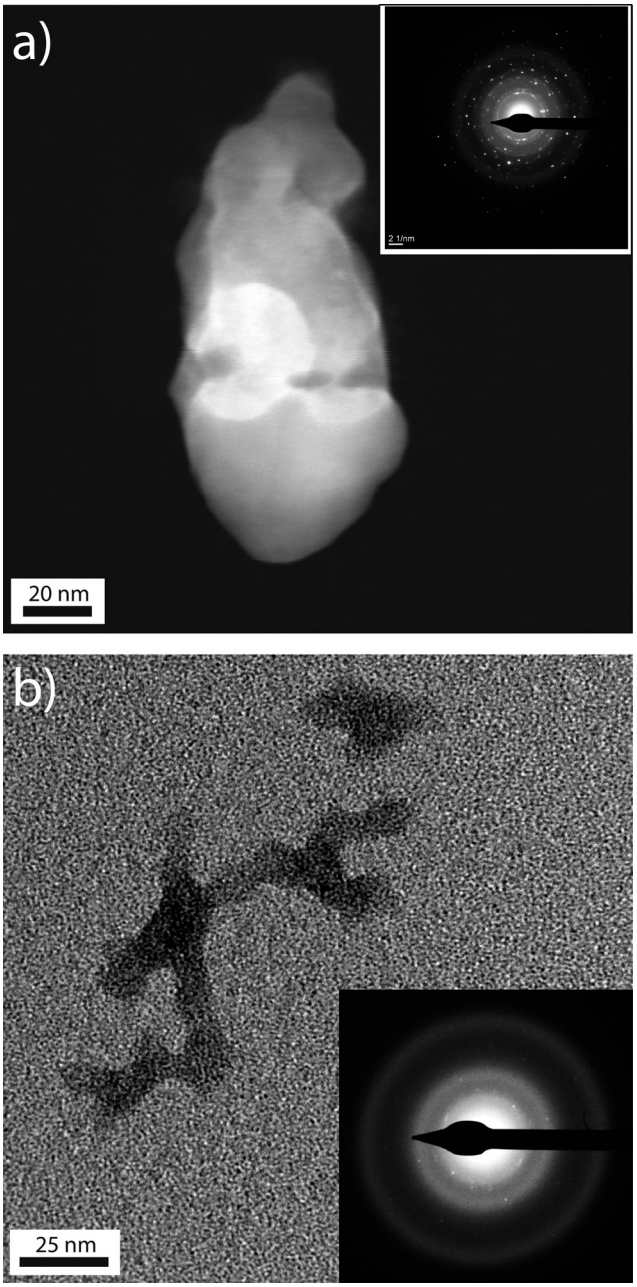

Fig. 5 Particles obtained after the isolation of the second aliquot in the 2.5 mg l^{-1} PAA titration experiment (second red arrow in Fig. 2). a) STEM-HAADF image of oval-shaped particles of approx. 100 nm. b) TEM photomicrograph of shapeless structures with not well-defined contours. Both SAED patterns show diffraction spots superimposed on diffuse halos that indicate the presence of amorphous material. EDX analysis confirmed the presence of Ba and S.

Characterization of barium sulphate precipitated by rapid mixing of reagent solutions

XRD patterns of freeze-dried $BaSO_4$ solids formed immediately upon mixing in the absence of PAA show already well defined, though wide and low-intensity, peaks corresponding to 111, 210, 102, 211, 112, 202 Bragg peaks of barite (Fig. 7). Interestingly, this is not seen in the presence of PAA in samples quenched immediately upon mixing; instead, a broad band located at 10–35° 2θ is observed. XRD patterns of PAA-doped samples quenched after 20 seconds of mixing eventually show the emergence of very broad bands centred at ~20.0, 22.5, 26.5, 29.0 and 32.5° 2θ (Fig. 7). From the

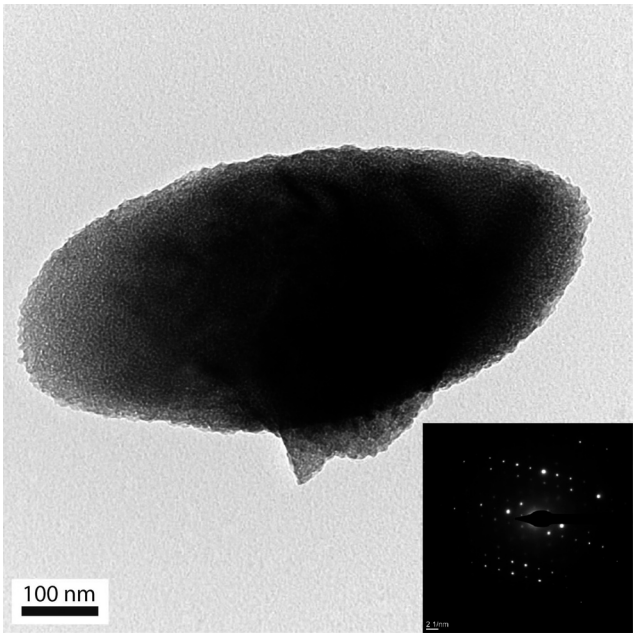

Fig. 6 TEM photomicrograph of the last sample taken in the 2.5 mg l^{-1} PAA titration experiment (third red arrow in Fig. 2). Barite rounded particles formed by smaller subunits are observed at this stage. These rounded particles diffract as single crystals (SAED in lower right corner). EDX analysis and *d*-spacing in the SAED pattern confirm they are barite.

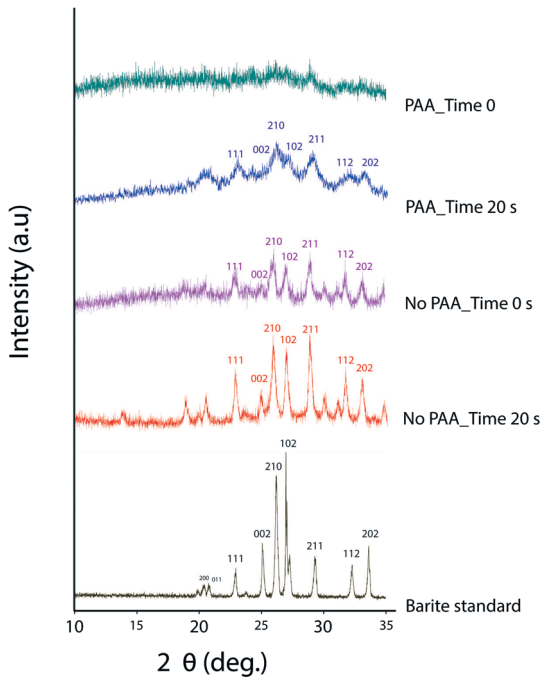

Fig. 7 XRD patterns of freeze-dried $BaSO_4$ solids obtained immediately after mixing of reagent solution (0 s) and after incubation for 20 s in solution, in the presence and in the absence of PAA. The lower black pattern corresponds to an equal volume of pure, natural barite powder.

comparison of the intensities of the different crystallographic peaks with those of an equal volume of pure, natural barite (black pattern in Fig. 7), a clear evolution of the crystallinity of the precipitated material with increasing incubation time in solution before quenching can be seen. In all cases, the intensities of X-ray reflections obtained from the samples prepared by rapid mixing of $Ba(OH)_2$ and H_2SO_4 solutions, in the absence and in the presence of PAA, (Fig. S7 and S6, ESI†) were much lower than those obtained from the same volume of a natural barite powder; this is a clear indication of the existence of an amorphous or poorly crystalline phase, as has been stated for other amorphous phases such as amorphous calcium carbonate (ACC).[25]

Three distinct stages are observed in TGA plots of freeze-dried pure and PAA-bearing $BaSO_4$ samples collected at different times upon mixing of $Ba(OH)_2$ and H_2SO_4 solutions (Fig. S7, ESI†). There is an initial weight loss from room *T* up to ~155 °C, associated with desorption of physically adsorbed water.[26] The weight loss occurring from 155 to 455 °C is due to the decomposition of chemically adsorbed water and the partial decomposition of hydroxide groups.[26] Subsequent weight loss from 455 to 950 °C is related to further decomposition of hydroxide groups.[26] TGA of pure $BaSO_4$ samples incubated in solution for different times clearly showed a progressive reduction in the water-associated weight loss from 7.70 wt% at t = 0 down to 7.39 wt% at t = 20 s and 7.18 wt% at t = 1 h, expressed as grams lost per 100 grams of pure, dry $BaSO_4$. In the presence of PAA, this effect is also observed (weight loss: 11.60 wt% at t = 0 down to 10.48 wt% at t = 20 s and 9.65 wt% at t = 1 h). Although the decomposition of PAA partially overlaps with $BaSO_4$ dehydration, as the amount of PAA is constant in the powder, the progressive reduction in the weight loss is ascribed to a progressive dehydration of $BaSO_4$ particles with the time of incubation in the growth media.

After XRD analysis, freeze-dried samples were studied by ESEM, TEM and FESEM. Samples were kept in a dry environment (a silica-gel container) to avoid any phase transition; however, it seems that some transformation took place as shown by our TEM and FESEM images. Fig. 8 shows TEM images of the initial precipitates (quenched immediately upon mixing of the $Ba(OH)_2$ and H_2SO_4 solutions). $BaSO_4$ precipitated in the absence of polymer appears both as individual, isolated crystals, that display mostly rounded or oval shapes (Fig. 8a), and micron-sized aggregates in the form of rosettes known as 'desert roses' in natural barite (Fig. 8b). Each desert rose seems to comprise several of the isolated oval crystals. Rarely, individual $BaSO_4$ particles appear as porous aggregates. SAED patterns of these aggregates show diffraction spots superimposed into weak rings confirming the coexistence of nanocrystals with an amorphous $BaSO_4$ phase (Fig. 8c). PAA does not seem to significantly alter the overall morphology of $BaSO_4$ precipitates under our experimental conditions. Nevertheless, oval-shaped $BaSO_4$ particles are in this case mostly porous aggregates of crystallographically oriented barite nanoparticles that diffract as mesocrystals (Fig. 8d). FESEM observations (Fig. 9) show rounded and oval-shaped micron-sized $BaSO_4$ particles in both pure and PAA-bearing samples. The surface of these crystals appears

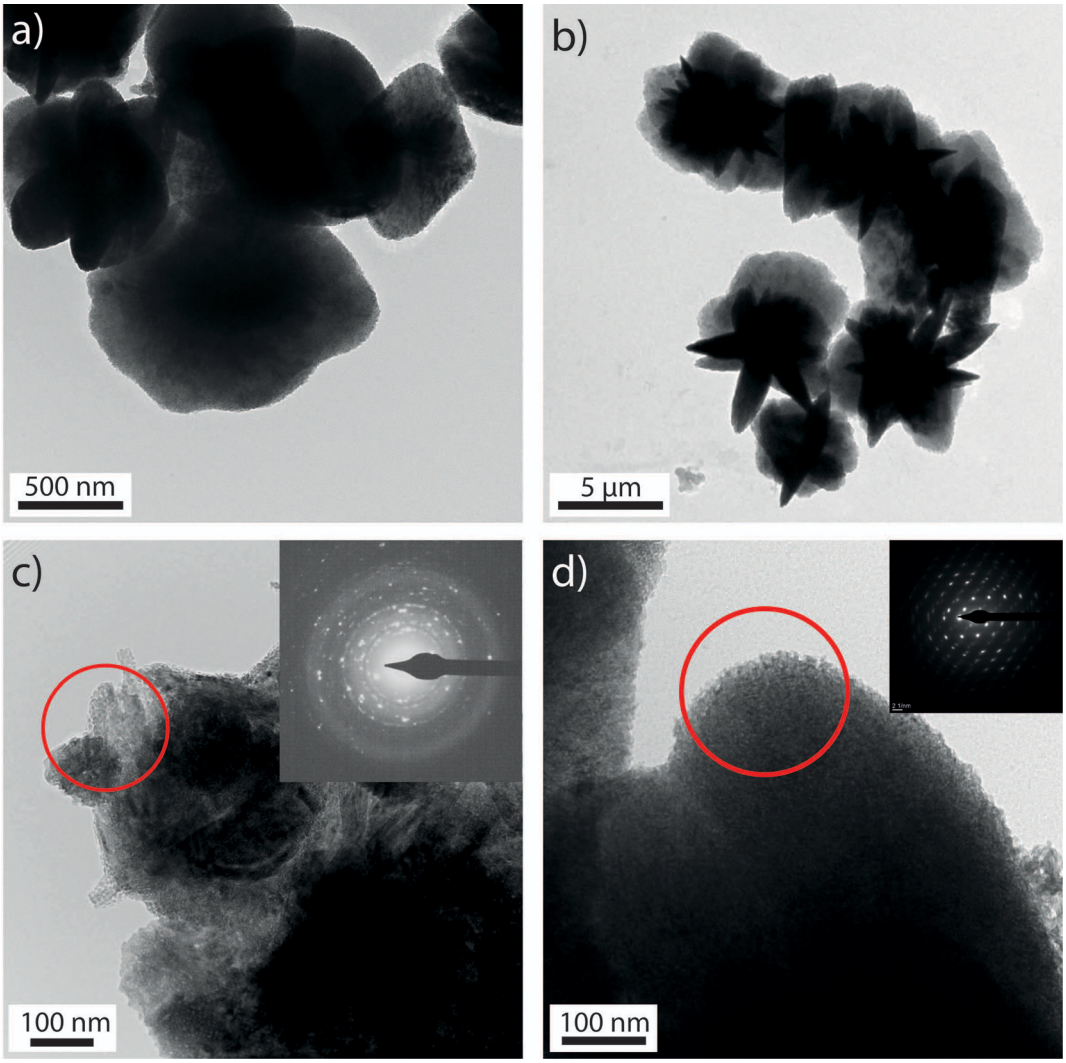

Fig. 8 TEM photomicrograph of the initial precipitates (quenched immediately upon mixing of the $Ba(OH)_2$ and H_2SO_4 solutions). $BaSO_4$ precipitated in the absence of polymer are mostly a) rounded- or oval-shaped, b) micron-sized aggregates in the form of rosettes, and c) individual porous aggregates of $BaSO_4$ nanoparticles. SAED patterns (insets) show diffraction spots superimposed onto weak rings. d) In the presence of PAA oval-shaped $BaSO_4$ particles are mostly porous aggregates of crystallographically oriented barite nanoparticles that diffract as mesocrystals (SAED in inset).

rough, confirming that crystals are actually aggregates of nanometer-sized particles.

Together with the rounded particles seen in the FESEM images, ESEM observations (Fig. 10) of freeze-dried samples show abundant $BaSO_4$ structures with fibrous or planar shapes in both pure and PAA-bearing samples that were not seen under the FESEM or TEM. Additionally, shapeless $BaSO_4$ structures are seen in the PAA-bearing samples, and nanocrystals appear inlaid in an apparently amorphous matrix, possibly corresponding to the organic compound (red arrows in Fig. 10b). These samples are not carbon-coated and are observed under low vacuum, thus guaranteeing a minimum alteration of the microstructure of the phase formed during the precipitation process. Note that similar 1D and 2D structures have been also obtained during the synthesis of $CaCO_3$.[6] Much smaller, apparently rounded isolated nanoparticles were also seen in the PAA-bearing samples. Finally, the same rounded and oval morphologies observed in the TEM, ESEM and FESEM images were seen in air under AFM upon deposition of ethanol suspensions of freeze-dried powders on glass slides (Fig. S7, ESI†). The thicknesses of these particles range from 2 to 30 nm, with diameters (assuming approximately rounded morphologies) ranging from 10 to 250 nm. This confirms the plate-like morphology of the $BaSO_4$ particles.

Discussion

Prenucleation stage in pure systems

Barite crystallization has been recently shown to occur *via* non-classical crystallization pathways, including the formation of a dense liquid precursor phase and the oriented

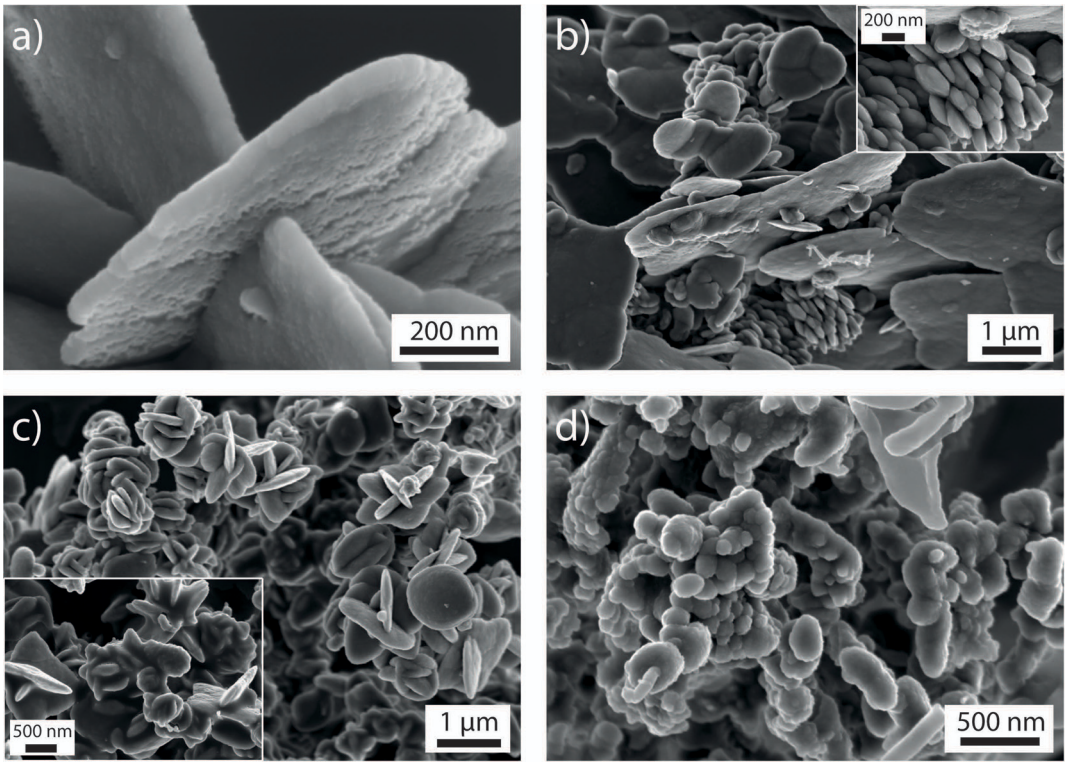

Fig. 9 FESEM images of freeze-dried precipitates quenched at different times. a) Pure sample (PAA-free) quenched at time ~0 s. b) Pure sample quenched at time ~20 s (detail of nanoparticle aggregate in inset). c) PAA-bearing sample quenched at time ~0 s. d) PAA-bearing sample quenched at time ~20 s.

attachment of nano-crystalline primary particles.[4] Our results add to these previous findings and suggest that Ba^{2+} and SO_4^{2-} ions undergo association to form stable complexes prior to liquid–liquid separation and solid barium sulphate nucleation, as reported previously for other sparingly soluble minerals such as $CaCO_3$ (ref. 21) and $BaCO_3$.[22]

The formation of ion associates (pairs and/or larger clusters) prior to nucleation thus seems to be a widespread feature of many mineral precipitation processes. The amount of barium bound to sulphate in the $BaSO_4$ prenucleation stage (between 70–80% at nucleation point) is significantly higher than the fraction of Ba^{2+} and comparable to the Ca^{2+} bound to carbonate determined in previous work (about 32%[22] and 75%[21] bound at pH 10 for barium carbonate and calcium carbonate, respectively). This suggests that $BaSO_4$ prenucleation species are more stable than $BaCO_3$ or even $CaCO_3$ clusters. Although the exact mechanism for this behavior remains unknown, we can speculate that it could be related to the kosmotrope (structure maker) character of the sulphate ion.[27]

Prenucleation species should be regarded as polynuclear associates of solute ions with a highly dynamic character; they are continuously disassembling into smaller clusters and/or ion pairs and re-aggregating.[28] As an isolated ion, sulphate is coordinated to an average of 12 water molecules by H-bonding. Additionally, the mean residence time of water ligands at oxygen atoms of the sulphate ion is longer than that in bulk water.[27] A similar behaviour is thus expected once sulphate is in ion pairs and/or clusters. If we assume that for dis-assembling the prenucleation species water bonds need to be broken, then the presence of sulphate ions in these clusters could slow down the dynamics of the ion pairs and/or cluster equilibrium, apparently enhancing association of Ba^{2+} and SO_4^{2-} ions and increasing the stability of the prenucleation species.

Once a certain ion activity product in solution is reached, prenucleation species can increase their level of coordination and density and become less dynamic; these larger, dense clusters will thus tend to remain as aggregates, without showing interfacial surfaces.[29] There may be certain configurations that may be more stable than others, also slowing down the dynamics of ion pairs and/or prenucleation clusters.[29] Clusters may also grow in size by aggregation.[30] This may occur up to a point when these large prenucleation species develop interfaces, and become nanodroplets. Such a change in speciation may indeed be regarded as liquid–liquid separation. Moreover, the nanodroplets can aggregate and form larger species with a liquid-like character as well.[28] In this way, how a dense liquid precursor phase forms from a molecular point of view can be explained.[28] Such a mechanism would link the present findings with our previously reported observations regarding the formation of a dense liquid phase prior to solid $BaSO_4$ nucleation.[4] Some time later, the larger liquid entities undergo progressive dehydration and,

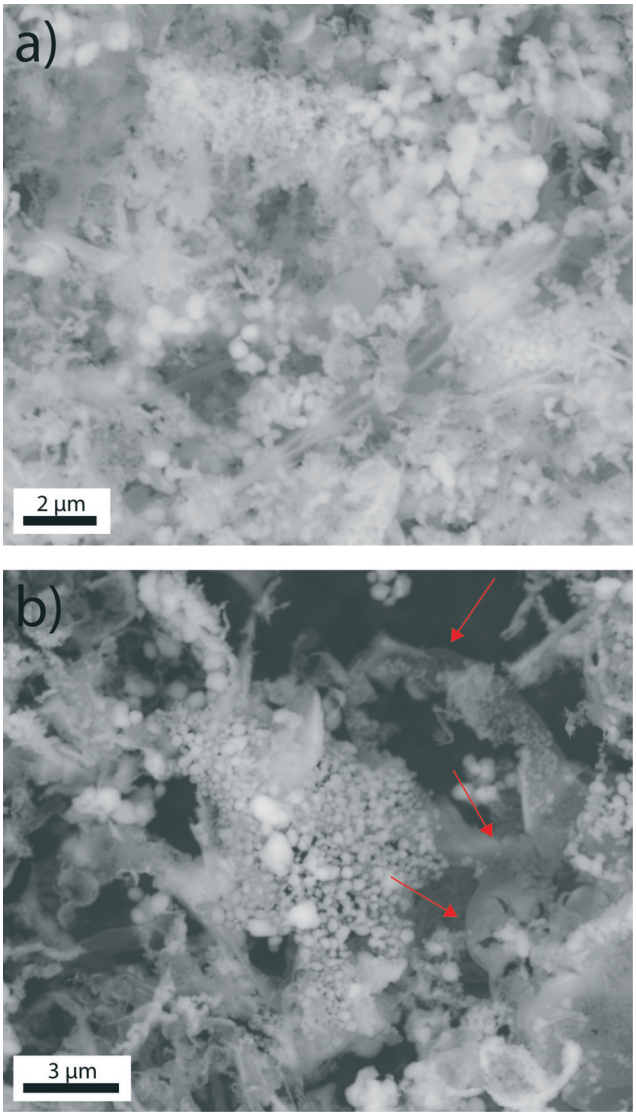

Fig. 10 $BaSO_4$ structures with fibrous or planar shapes in both a) pure and b) PAA-bearing freeze-dried samples observed under ESEM.

eventually, solid nanoparticles nucleate within this dense liquid precursor phase.

Solid amorphous $BaSO_4$ as a precursor to crystalline barite

Previous studies on the early stages of barium sulphate formation in pure systems have not conclusively resolved the existence or not of an amorphous solid precursor to crystalline barite.[10] Our previous findings (*i.e.*, observation of rounded morphologies of the initial solid nanoparticles or the detection in the assemblages of nanoparticles of crystalline domains separated by areas that do not show lattice fringes) suggest than an amorphous phase may precede the formation of crystalline barite.[4] Indeed, the present TEM observations of time-resolved samples obtained in titration experiments confirm the existence of an amorphous solid phase previous to crystalline barite. Moreover, SAED patterns of freeze-dried $BaSO_4$ precipitates (Fig. 8) show weak, diffuse halos or rings corresponding to amorphous material together with scarce diffraction spots with *d*-spacings corresponding to barite, providing evidence for an amorphous to crystalline transition in the system. Finally, XRD analyses of freeze-dried $BaSO_4$ powders suggest that a significant proportion of amorphous material is present in the precipitates (Fig. S7 and S5, ESI†).

TG analyses (Fig. S6, ESI†) suggest that this amorphous barium sulphate phase, initially formed in counter-ion and organic-free aqueous solutions (*i.e.*, rapid mixing experiments), is hydrated. Moreover, these analyses show a progressive decrease in the water content in the solids from 1 to 0.9 moles of H_2O per formula unit after 60 minutes of incubation. The formation of a less hydrated amorphous barium sulphate phase over time spent in solution is interpreted as a progressive dehydration of $BaSO_4$ precipitates in solution. Because of the intrinsic instability of amorphous intermediates relative to the crystalline phases, the chance of detecting the formation of amorphous precursors depends on their lifetime.[5] Amorphous phases frequently contain hydration water and the formation of anhydrous crystalline phases involves expelling this hydration water.[9] Amorphous phases in Ca- or Mg-bearing compounds are expected to be relatively stable compared to Ba-bearing systems due to the strongly hydrated character of Ca^{2+} and Mg^{2+} compared to Ba^{2+}. Given the fact that the energy barrier for the amorphous to crystalline transition in this system may be small, the existence of a short-lived intermediate species may well have been overlooked in pure systems. Moreover, the lifetime of these transient phases is progressively shortened with increasing supersaturation of the solution from which they precipitate. The initially formed amorphous nanoparticles may crystallize and grow *via* different levels of oriented aggregation as shown in our previous work.[4]

Effect of poly(acrylic acid) on $BaSO_4$ precipitation

As stated above, the results from titration experiments suggest that a dynamic equilibrium of stable ion complexes exists in solution before the onset of phase separation. The slope of the free barium development curve in the linear range gives information of prenucleation species formation and their stability.[23] Changes in this slope in the presence of additives or impurities are related to interactions of such compounds with $BaSO_4$ ion associates in solution, influencing the extent of formation and/or the structure of soluble barium sulphate prenucleation species.[20] The observed steeper slope with increasing PAA concentration indicates that less barium is incorporated in these clusters when PAA is present relative to the reference (*i.e.* PAA-free) case. Similarly, it has been shown that an increase in ionic strength in the solution causes also a steeper slope of free-Ca^{2+}-concentration curve due to the reduced activity of free calcium and carbonate ions which leads to a lower amount of ions bound in pre-nucleation associates.[20] Thus, it seems

that the presence of PAA in the barium sulphate system somehow destabilizes the prenucleation species formed making them less stable. Similar observations have been recently made for calcium carbonate formation in the presence of poly(aspartic) acid and magnesium.[31] In this case, no molecular explanation is given for the observed destabilization of the calcium/magnesium carbonate prenucleation clusters in the presence of poly(aspartic) acid; however, it is concluded that it contributes to the synergetic inhibitory effect of Mg and PAA on $CaCO_3$ precipitation.

For our system, molecular dynamics simulations have shown that acidic molecules such as aspartic acid indeed enhance the rate of Ba^{2+} desolvation in the $BaSO_4$–H_2O system.[32] Thus, although we can only speculate about a possible molecular explanation for the observed lower stability of prenucleation species in the presence of PAA, it appears reasonable to propose that, as with other acidic bio-molecules, it may aid in desolvating barium and $BaSO_4$ complexes/clusters. As explained above, in the $BaSO_4$–H_2O system a weaker hydration could increase the dynamics of the ion pairs and/or clusters equilibrium and destabilize pre-nucleation species. Enhanced ion desolvation by acidic bio-molecules has been invoked, for example, to explain the increase in Mg uptake by calcite during growth in the presence of peptides[33] or alcohol.[34]

Moreover, this effect is accompanied by a delay in nucleation relative to the reference case (absence of PAA). At a PAA concentration of 50 mg l^{-1}, the slope of the curve is almost equal to that of the added barium and thus the formation of prenucleation clusters compared to reference experiments would be negligible. At this concentration, nucleation is completely inhibited for at least 20 hours. Thus, these results indirectly confirm that the formation and subsequent aggregation of ion pairs and/or clusters are required steps for $BaSO_4$ nucleation. The low binding capacity of the PAA (that increases with increasing PAA concentration) was found to be *ca.* one barium ion to *ca.* 5 carboxylic acid groups, and thus does not seem a feasible mechanism for barite inhibition by PAA. According to our results, it appears more likely that the main mechanism by which PAA inhibits $BaSO_4$ formation under the given conditions is related to destabilization possibly related to organic molecule incorporation) of prenucleation species. In the presence of PAA, less barium (and sulphate) is bound within pre-nucleation clusters and nucleation is inhibited compared to the pure system (*i.e.*, no PAA). Additionally, the increase in solubility of the precipitated phase again points to possible PAA incorporation likely in an amorphous or poorly crystalline precursor (as seen in the higher free barium concentration in solution in equilibrium with the initially precipitated phase: see Fig. 2) and could also contribute to the observed delay in the onset of the precipitation process.

In those experiments where full inhibition is not achieved (*i.e.*, for PAA concentrations lower than 50 mg l^{-1}), the formation of Ba-PAA globules in solution provides an alternative route for $BaSO_4$ mineralization, and helps to disclose the mechanism of polymer additive-$BaSO_4$ interaction. According to our TEM (Fig. 4) and EDX analyses (Fig. S3, ESI†), in these cases it can be argued that PAA molecules encapsulate barium ions and subsequently barium sulphate precipitates from these Ba-PAA globules. Changes in the conformation of PAA in aqueous solutions with increasing concentration of divalent cations such as Sr^{2+} have been reported.[35] Divalent strontium binds to the carboxylate groups neutralizing the negative charge of the PAA chain, which results in the collapse of the hydrophobic polymer chain that adopts a "pearl necklace" structure, trapping Sr^{2+} ions.[7] A similar process could also happen to PAA chains when a certain level of barium concentration in solution is reached and Ba-PAA globules will then form (Fig. 4). The formation of these Ba-rich globules could explain the fact that a drop in free-Ba^{2+} concentration is observed before the decrease in transmittance (Fig. 2b), probably because these globules are solutes, with no interface between these structures and the bulk solution. Similar observations have been recently reported for calcium carbonate nucleation and growth in a matrix of polystyrene sulphonate[36] showing that the negatively charged polystyrene sulphonate acts as a sponge that binds calcium ions and locally concentrates them. The existence of these Ba-PAA complexes was deduced from analytical ultracentrifugation by Wang and Cölfen;[13] however, our TEM analysis resolve the detailed nature, size and composition of these globules. In addition, our experiments demonstrate that these Ba-PAA globules also form when sulphate ions are present in solution.

Nevertheless, the formation of PAA-globules could be a kinetically dominant process with PAA molecules being excluded with time as sulphate species compete with the polymer for its bound barium. Eventually, amorphous barium sulphate nucleates around and within these globules (Fig. 5). These $BaSO_4$ particles immediately crystallize upon irradiation under the electron beam. However, diffuse halos or rings are still seen in the SAED patterns, indicating the presence of amorphous material in these particles. The fact that diffraction spots are superimposed on the rings suggests that the amorphous phase may have a barite proto-structure (Fig. 5b). At this stage, a drop in both transmittance and conductivity of the solution is observed while barium decreases slower (region (II) in Fig. S2, ESI†); the removal of Ba^{2+} due to solid $BaSO_4$ formation is faster than $BaCl_2$ addition and thus the net effect is a decrease in conductivity.

Finally, oval-shape $BaSO_4$ particles that diffract as single barite crystals form in solution (Fig. 6). Even though the SAED pattern corresponds to a barite single crystal, it can be clearly seen that the particle is formed by smaller subunits that are crystallographically oriented. At this stage, the precipitation rate has significantly slowed down, as deduced from the slope of the free Ba^{2+} concentration curves (region (III) in Fig. S2, ESI†). In a previous work,[14] bundles of barite fibres were obtained in the presence of PAA (5100 mg mol^{-1}) as a result of oriented aggregation of $BaSO_4$ subunits. Under our experimental conditions such morphologies are not

found and only rounded barite particles were observed, presumably also formed by the oriented aggregation of $BaSO_4$ nanoparticles. The fact that the individual nanoparticles making the micrometre sized $BaSO_4$ structures are surrounded by low e-absorbing areas, which could be pores or zones were PAA concentrates, and are aligned in crystallographic register, as shown by the single-crystal features of the SAED pattern, confirm that these structures are mesocrystals.

Conclusions

The results presented here strongly support the concept that the early stages of $BaSO_4$ crystallization involve the formation of ion associates (pairs and/or clusters) in the prenucleation regime. The percentage of bounded barium ions at the nucleation point is comparable to the well-studied $CaCO_3$ case, and significantly higher than in the case of $BaCO_3$. In the presence of PAA, these prenucleation species seem to be destabilized and, concomitantly, nucleation is progressively delayed. Importantly, these results provide experimental evidence that the formation of prenucleation ion associates or clusters is a required step for nucleation. Additionally, this work gives insights into the mechanism of scale formation inhibition by polyelectrolytes and may aid in the selection of more effective additives for such purposes. Once the "prenucleation species" route is inhibited in the presence of the required amount of PAA, an alternative route for barite precipitation occurs which involves the initial formation of Ba-PAA globules. Secondly, sulphate ions displace PAA and an amorphous $BaSO_4$ phase, apparently with a barite-like proto-structure, eventually forms from these globules. Such an amorphous (hydrated) barium sulphate phase also forms in salt-free solutions; the presence of organics such as PAA (or mellitic acid[10]) seems to increase the stability of this transient phase, thus allowing its identification and complete characterization. Subsequently, this phase transforms into crystalline barite nanoparticles upon dehydration. These barite nanoparticles aggregate in an oriented manner to form $BaSO_4$ mesocrystals that incorporate some amount of PAA.

Thus, the $BaSO_4$–H_2O system is another example of the precipitation of a crystalline phase *via* prenucleation aggregates and amorphous (liquid and solid) precursors, showing the universal character of these non-classical processes during crystallization of sparingly soluble minerals. The observation of these metastable phases probably has been precluded due to their short life-time. Moreover, our findings confirm the key role that acidic macromolecules may play during barite biomineralization in marine environments, already modulating the precipitation of $BaSO_4$ in the prenucleation regime. Finally, this work highlights the importance of employing synthesis (*i.e.*, freeze-drying) and characterization (*e.g.*, ESEM) methods that allow investigation of the earliest stages of nucleation and growth in systems with labile pre- and post-nucleation phases.

Acknowledgements

This research was carried out within a Marie Curie initial training network from the European Commission (MINSC ITN 290040). The Deutsche Forschungsgemeinschaft (DFG) supports the research at the University of Münster. E. Ruiz-Agudo acknowledges funding from the Spanish Government (grant MAT2012-37584) and the Junta de Andalucía (research group RNM-179 and project P11-RNM-7550-ERDF funds), as well as the receipt of a Ramón y Cajal grant from the Spanish Government (Ministerio de Economía y Competitivad). C. Rodriguez-Navarro acknowledges funding from the Spanish Government (grant CGL2012-35992). We would like to also thank the personnel of the "Centro de Instrumentación Científica" (University of Granada) for their support and help with the TEM and FESEM analyses.

References

1 M. Bader, Sulfate Removal Technologies for Oil Fields Seawater Injection Operations, *J. Pet. Sci. Eng.*, 2007, **55**, 93–110.
2 K. Sorbie and E. Mackay, Mixing of Injected, Connate and Aquifer Brines in Waterflooding and its Relevance to Oilfield Scaling, *J. Pet. Sci. Eng.*, 2000, **27**, 85–106.
3 M. T. Gonzalez-Muñoz, B. Fernandez-Luque, F. Martínez-Ruiz, K. B. Chekroun, J. M. Arias, M. Rodríguez-Gallego, M. Martínez-Canamero, C. de Linares and A. Paytan, Precipitation of Barite by Myxococcus xanthus: Possible Implications for the Biogeochemical Cycle of Barium, *Appl. Environ. Microbiol.*, 2003, **69**, 5722–5725.
4 C. Ruiz-Agudo, E. Ruiz-Agudo, C. V. Putnis and A. Putnis, Mechanistic Principles of Barite Formation: From Nanoparticles to Micron-Sized Crystals, *Cryst. Growth Des.*, 2015, **15**, 3724–3733.
5 Y.-W. Wang, Y.-Y. Kim, H. K. Christenson and F. C. Meldrum, A New Precipitation Pathway for Calcium Sulfate Dihydrate (Gypsum) Via Amorphous and Hemihydrate Intermediates, *Chem. Commun.*, 2012, **48**, 504–506.
6 C. Rodriguez-Navarro, K. Kudłacz, Ö. Cizer and E. Ruiz-Agudo, Formation of Amorphous Calcium Carbonate and its Transformation into Mesostructured Calcite, *CrystEngComm*, 2015, **17**, 58–72.
7 A. V. Dobrynin, M. Rubinstein and S. P. Obukhov, Cascade of Transitions of Polyelectrolytes in Poor Solvents, *Macromolecules*, 1996, **29**, 2974–2979.
8 R. Schmid, A. M. Miah and V. N. Sapunov, A New Table of The Thermodynamic Quantities of Ionic Hydration: Values and Some Applications (Enthalpy–Entropy Compensation and Born Radii), *Phys. Chem. Chem. Phys.*, 2000, **2**, 97–102.
9 J. H. E. Cartwright, A. G. Checa, J. D. Gale, D. Gebauer and C. I. Sainz-Díaz, Calcium Carbonate Polyamorphism and Its Role in Biomineralization: How Many Amorphous Calcium Carbonates Are There?, *Angew. Chem., Int. Ed.*, 2012, **51**, 11960–11970.

10 F. Jones, Infrared Investigation of Barite and Gypsum Crystallization: Evidence for An Amorphous to Crystalline Transition, *CrystEngComm*, 2012, **14**, 8374–8381.
11 S.-H. Yu, M. Antonietti, H. Cölfen and J. Hartmann, Growth and Self-Assembly of $BaCrO_4$ and $BaSO_4$ Nanofibers toward Hierarchical and Repetitive Superstructures by Polymer-Controlled Mineralization Reactions, *Nano Lett.*, 2003, **3**, 379–382.
12 H. Cölfen, Double-Hydrophilic Block Copolymers: Synthesis and Application as Novel Surfactants and Crystal Growth Modifiers, *Macromol. Rapid Commun.*, 2001, **22**, 219–252.
13 T. Wang and H. Cölfen, In Situ Investigation of Complex $BaSO_4$ Fiber Generation in the Presence of Sodium Polyacrylate. 1. Kinetics and Solution Analysis, *Langmuir*, 2006, **22**, 8975–8985.
14 T. Wang, A. Reinecke and H. Cölfen, In Situ Investigation of Complex $BaSO_4$ Fiber Generation in the Presence of Sodium Polyacrylate. 2. Crystallization Mechanisms, *Langmuir*, 2006, **22**, 8986–8994.
15 D. Gebauer, H. Cölfen, A. Verch and M. Antonietti, The Multiple Roles of Additives in $CaCO_3$ Crystallization: A Quantitative Case Study, *Adv. Mater.*, 2009, **21**, 435–439.
16 S. Mann, Biomineralization, *Principles and Concepts in Bioinorganic Materials Chemistry*, 1st edn, 2001.
17 L. B. Gower and D. J. Odom, Deposition of Calcium Carbonate Films by A Polymer-Induced Liquid-Precursor (PILP) Process, *J. Cryst. Growth*, 2000, **210**, 719–734.
18 S. Bentov, S. Weil, L. Glazer, A. Sagi and A. Berman, Stabilization of Amorphous Calcium Carbonate by Phosphate Rich Organic Matrix Proteins and by Single Phosphoamino Acids, *J. Struct. Biol.*, 2010, **171**, 207–215.
19 Y.-W. Wang and F. C. Meldrum, Additives Stabilize Calcium Sulfate Hemihydrate (Bassanite) in Solution, *J. Mater. Chem.*, 2012, **22**, 22055.
20 M. Kellermeier, A. Picker, A. Kempter, H. Cölfen and D. Gebauer, A Straightforward Treatment of Activity in Aqueous $CaCO_3$ Solutions and the Consequences for Nucleation Theory, *Adv. Mater.*, 2014, **26**, 752–757.
21 D. Gebauer, A. Völkel and H. Cölfen, Stable Prenucleation Calcium Carbonate Clusters, *Science*, 2008, **322**, 1819–1822.
22 J. Eiblmeier, U. Schürmann, L. Kienle, D. Gebauer, W. Kunz and M. Kellermeier, New Insights into the Early Stages of Silica-Controlled Barium Carbonate Crystallisation, *Nanoscale*, 2014, **6**, 14939–14949.
23 A. Verch, D. Gebauer, M. Antonietti and H. Cölfen, How to Control The Scaling of $CaCO_3$: A "Fingerprinting Technique" to Classify Additives, *Phys. Chem. Chem. Phys.*, 2011, **13**, 16811–16820.
24 J. Ihli, A. N. Kulak and F. C. Meldrum, Freeze-Drying Yields Stable and Pure Amorphous Calcium Carbonate (ACC), *Chem. Commun.*, 2013, **49**, 3134.
25 E. Beniash, J. Aizenberg, L. Addadi and S. Weiner, Amorphous Calcium Carbonate Transforms into Calcite During Sea Urchin Larval Spicule Growth, *Proc. R. Soc. London, Ser. B*, 1997, **264**, 461–465.
26 H. Bala, W. Fu, Y. Guo, J. Zhao, Y. Jiang, X. Ding, K. Yu, M. Li and Z. Wang, In Situ Preparation and Surface Modification of Barium Sulfate Nanoparticles, *Colloids Surf., A*, 2006, **274**, 71–76.
27 V. Vchirawongkwin, B. M. Rode and I. Persson, Structure and Dynamics of Sulfate Ion in Aqueous Solutions–An ab initio QMCF MD Simulation and Large Angle X-ray Scattering Study, *J. Phys. Chem. B*, 2007, **111**, 4150–4155.
28 D. Gebauer, M. Kellermeier, J. D. Gale, L. Bergström and H. Cölfen, Pre-Nucleation Clusters as Solute Precursors in Crystallisation, *Chem. Soc. Rev.*, 2014, **43**, 2348–2371.
29 A. R. Finney and P. M. Rodger, Probing The Structure and Stability of Calcium Carbonate Pre-Nucleation Clusters, *Faraday Discuss.*, 2012, **159**, 47–60.
30 M. Kellermeier, D. Gebauer, E. Melero-García, M. Drechsler, Y. Talmon, L. Kienle, H. Cölfen, J. M. García-Ruiz and W. Kunz, Colloidal Stabilization of Calcium Carbonate Prenucleation Clusters with Silica, *Adv. Funct. Mater.*, 2012, **22**, 4301–4311.
31 S. L. P. Wolf, K. Jähme and D. Gebauer, Synergy of Mg^{2+} and Poly(Aspartic Acid) in Additive-Controlled Calcium Carbonate Precipitation, *CrystEngComm*, 2015, **17**, 6857–6862.
32 S. Piana, F. Jones and J. D. Gale, Assisted Desolvation as a Key Kinetic Step for Crystal Growth, *J. Am. Chem. Soc.*, 2006, **128**, 13568–13574.
33 A. E. Stephenson, J. J. De Yoreo, L. Wu, K. J. Wu, J. Hoyer and P. M. Dove, Peptides Enhance Magnesium Signature in Calcite: Insights into Origin of Vital Effects, *Science*, 2008, **322**, 724–727.
34 G. Falini, M. Gazzano and A. Ripamonti, Magnesium Calcite Crystallization from Water-Alcohol Mixtures, *Chem. Commun.*, 1996, 1037–1038.
35 G. Goerigk, R. Schweins and K. Huber, Evidence for Pearl-Necklace Structure in Aqueous Solution of Polyacrylate Chains with Sr^{2+}-Counterions, *Europhys. Lett.*, 2004, **66**, 331–337.
36 P. J. M. Smeets, K. R. Cho, R. G. E. Kempen, N. A. J. M. Sommerdijk and J. J. de Yoreo, Calcium Carbonate Nucleation Driven by Ion Binding in a Biomimetic Matrix Revealed By In Situ Electron Microscopy, *Nat. Mater.*, 2015, **14**, 394–399.

